Hindawi
Journal of Nanomaterials
Volume 2018, Article ID 9509126, 9 pages
https://doi.org/10.1155/2018/9509126

Research Article

Enhancement of Capacitive Performance in Titania Nanotubes Modified by an Electrochemical Reduction Method

Nurul Asma Samsudin,[1] **Zulkarnain Zainal**,[1,2] **Hong Ngee Lim**,[1,2] **Yusran Sulaiman**,[1,3] **Sook-Keng Chang**,[2] **Ying-Chin Lim**,[4] **and Wardatun Nadrah Mohd Amin**[1]

[1]*Department of Chemistry, Faculty of Science, Universiti Putra Malaysia, 43400 Serdang, Selangor, Malaysia*
[2]*Materials Synthesis and Characterization Laboratory, Institute of Advanced Technology, Universiti Putra Malaysia, 43400 Serdang, Selangor, Malaysia*
[3]*Functional Devices Laboratory, Institute of Advanced Technology, Universiti Putra Malaysia, 43400 Serdang, Selangor, Malaysia*
[4]*School of Chemistry and Environment, Faculty of Applied Science, Universiti Teknologi MARA, 40450 Shah Alam, Selangor, Malaysia*

Correspondence should be addressed to Zulkarnain Zainal; zulkar@upm.edu.my

Received 11 November 2017; Accepted 11 December 2017; Published 4 January 2018

Academic Editor: Xuping Sun

Highly ordered titania nanotubes (TNTs) were synthesised by an electrochemical anodization method for supercapacitor applications. However, the capacitive performance of the TNTs was relatively low and comparable to the conventional capacitor. Therefore, in order to improve the capacitive performance of the TNTs, a fast and facile electrochemical reduction method was applied to modify the TNTs (R-TNTs) by introducing oxygen vacancies into the lattice. X-ray photoelectron spectroscopy (XPS) data confirmed the presence of oxygen vacancies in the R-TNTs lattice upon the reduction of Ti^{4+} to Ti^{3+}. Electrochemical reduction parameters such as applied voltage and reduction time were varied to optimize the best conditions for the modification process. The electrochemical performance of the samples was analyzed in a three-electrode configuration cell. The cyclic voltammogram recorded at 200 mV s^{-1} showed a perfect square-shaped voltammogram indicating the excellent electrochemical performance of R-TNTs prepared at 5 V for 30 s. The total area of the R-TNTs voltammogram was 3 times larger than the unmodified TNTs. A specific capacitance of 11.12 mF cm^{-2} at a current density of 20 μA cm^{-2} was obtained from constant current charge-discharge measurements, which was approximately 57 times higher than that of unmodified TNTs. R-TNTs also displayed outstanding cycle stability with 99% capacity retention after 1000 cycles.

1. Introduction

Global energy crisis, the depletion of fossil fuels, and the ever increasing environmental pollution have all led to an urgent search of efficient, clean, and sustainable alternative energy supply and storage. Moreover, due to the increased power demand worldwide, there has been a need to develop high power and high energy devices that are robust and are able to withstand hundreds and thousands of charging/discharging cycles without being degraded. In recent years, electrochemical capacitors, also known as ultracapacitors and supercapacitors, have attracted significant attention, mainly due to their promising properties: higher power density than batteries, higher energy density than conventional capacitors, fast charging-discharging rates, and prolonged cycle life [1]. Supercapacitors are characterized as electric double-layer capacitors (EDLC) and pseudocapacitors. Electrical energy storage in EDLC occurs at the phase boundary between the electrode (active material) and the electrolyte solution (liquid ionic conductor) [2] with no charge-transfer involvement. Electrodes that use the current generated by the displacement of current due to charge rearrangement are known as ideally polarized electrodes [3, 4]. As for pseudocapacitors, charge storage is caused by the fast faradaic redox reaction due to

Table 1: Voltage and time taken in the electrochemical reduction method of R-TNTs.

Label	Voltage (V), time (s)
R-TNTs 4V30s	4 V, 30 s
R-TNTs 5V30s	5 V, 30 s
R-TNTs 6V30s	6 V, 30 s
R-TNTs 7V30s	7 V, 30 s
R-TNTs 5V10s	5 V, 10 s
R-TNTs 5V20s	5 V, 20 s
R-TNTs 5V40s	5 V, 40 s

redox-active materials such as metal oxides and conducting polymers on the surface and in the bulk near the surface of the electrode [4, 5].

Nanostructured materials have drawn great interest in the field of supercapacitors as they offer a combination of nanoscale dimensions with highly defined geometry and high surface areas. Titania has been considered as the best candidate for many applications over the past few decades due to its remarkable properties and strikingly high potential for practical applications [6–9]. Recently, titania nanotubes have been of much interest in energy storage owing to their capacity of being able to offer large surface areas and greatly improved electron transfer pathways compared to nonoriented structures, which in turn led to a higher charge propagation in active materials [6, 10, 11]. Among the various methods reported for the synthesis of titania nanotubes, the electrochemical anodization method has been the most promising method as its offers suitably back-connected nanotubes on the Ti foil substrate which can be used directly as a binder-free supercapacitor electrode [12]. However, TNT electrodes suffer from very low specific capacitance (less than 1 mF cm^{-2}) due to their poor electrical conductivity, which are similar to conventional electric double-layer capacitors [13, 14].

The enhancement of the capacitive performance of the TNTs can be carried out by electrochemical approaches and thermal treatments. Salari et al. (2011) reported the remarkable specific capacitance of the modified TNTs by thermal treatment optimization under an argon atmosphere [13]. The annealing process in a low oxygen atmosphere induced the evolution of oxygen vacancies that improved the specific capacitance. They disclosed that the highest specific capacitance of 2.6 mF cm^{-2} was obtained at 600°C which was higher than the previously reported capacitance of TiO_2 (100–911 μF cm^{-2}) [6, 13]. Besides argon, Endut et al. reported a specific capacitance of 0.118 mF cm^{-2} for titania nanotubes optimized by thermal treatment in ammonia (NH_3) [15]. It was concluded that by reducing the Ti^{4+} to Ti^{3+} during NH_3 annealing, the electrochemical performance of the sample was enhanced.

However, a simple, fast and cost-effective approach in modifying the TNTs for enhancing their electrochemical properties is much more desirable. Macak et al. reported that the higher conductivity layer at the bottom of the titania nanotubes layers formed by a reductive doping process [16]. This simple electrochemical method could be carried out in ambient temperatures and required simple preparation steps. In the doping process, Ti^{4+} was reduced to Ti^{3+} which acted as a donor center resulting in a highly conducting barrier layer [16–19]. They claimed that only 1% of the Ti^{4+} in the titania nanotubes layers could be reduced to Ti^{3+} and the color change in the films from light grey to black was a side effect of the reductive doping process. In this study, the focus was on utilizing the electrochemical reduction method to fabricate R-TNTs that meet the requirements as effective electrodes for supercapacitor applications.

2. Materials and Methods

2.1. Preparation of Titania Nanotubes. Pure Ti foil (0.125 mm thick, 99.7% purity, Sigma Aldrich) was degreased by sonicating in acetone, isopropanol, and deionized (DI) water for 15 min each followed by subsequent etching in 3 M HNO_3 (65%, MERCK) for 10 min to form a fresh smooth surface. They were then rinsed with excess DI water and dried in air. The titania nanotubes were fabricated in a two-electrode electrochemical cell with high density graphite as the cathode and Ti foil as the anode. Ethylene glycol (EG) (99.8% purity, initial water content < 0.03 wt%, Fisher Scientific) solution containing 0.5 wt% NH_4F (FLUKA) and 5 vol.% of water was used as the electrolyte. Anodization was carried out at a constant voltage of 40 V for 1 hour using a direct current (DC) power supply (Consort Mini, Cleaver Scientific Ltd). The distance between both electrodes was fixed at 3 cm in all experiments. After the anodization, the samples were immediately rinsed with DI water and dried in air. Finally, the samples were calcined at 500°C in air for 2 h with a heating rate of 2°C min^{-1}.

2.2. Electrochemical Reduction of Titania Nanotubes. The electrochemical reduction of TNTs was also performed in the same two-electrode electrochemical cell with the TNTs as the cathode while the high density graphite electrode was the anode. A supporting electrolyte containing 0.5 M Na_2SO_4 (MERCK) was used, and the distance between the two electrodes was fixed at 3 cm. The sample preparation parameters are shown in Table 1.

2.3. Material Characterization and Electrochemical Measurements. The morphology and the microstructure of the samples were examined by field emission scanning electron microscopy (FESEM, JSM-7600F, JOEL, Japan). X-ray diffraction patterns of the samples were collected using an X-ray diffractometer (Shimadzu, D60000, Japan) with Cu Kα (λ = 1.5406 Å) radiation to investigate the phase and composition of the prepared samples. The chemical states of the prepared samples were investigated using X-ray photoelectron spectroscopy (XPS, PHI Quantera II).

The electrochemical performance of the prepared samples was evaluated by cyclic voltammetry (CV), galvanostatic charge-discharge tests, and electrochemical impedance spectroscopy (EIS) using an Autolab PGSTAT204/FRA32M module. All of the electrochemical analyses were carried out using a three-electrode cell system. A platinum wire and an Ag/AgCl (3 M KCl) electrode were used as the counter and

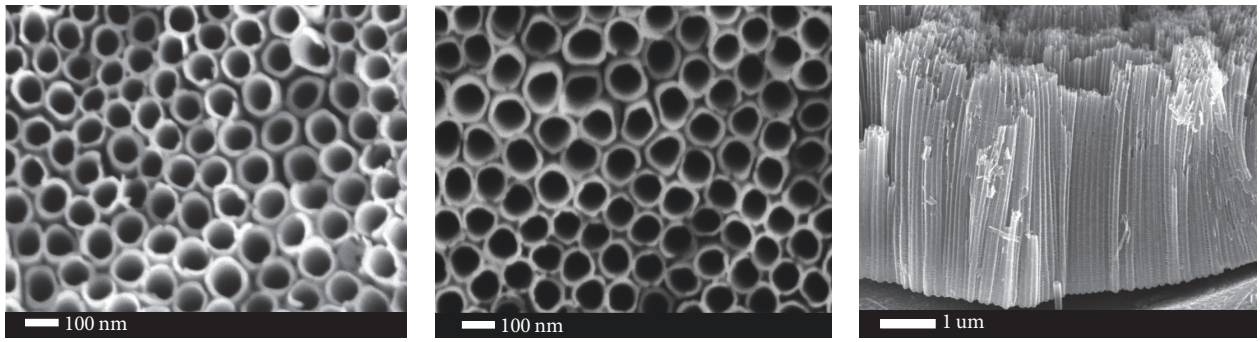

Figure 1: FESEM images of highly ordered (a) TNTs, (b) R-TNTs, and (c) a side view of the TNTs.

reference electrode, respectively, and the prepared samples were used as the working electrode. The prepared nanotube films were measured at an applied potential ranging from −0.4 V to 0.8 V versus Ag/AgCl in 1.0 M KCl aqueous electrolyte. The specific capacitance (SC) was calculated based on the charge-discharge curves using the following equation:

$$\mathrm{SC} = \frac{i \times \Delta t}{\Delta E \times A}, \tag{1}$$

where i is the discharge current in amperes, Δt is the discharge time in s, ΔE is the difference in discharge voltage in volts, and A is area of the active electrode in square centimetres. The stability of the R-TNTs was investigated up to 1000 cycles at a current density of 200 μA cm^{-2}.

3. Results and Discussion

3.1. Material Characterization. Figures 1(a) and 1(b) show the morphology of the TNTs and R-TNTs obtained from FESEM. The average geometrical size including the inner diameter, wall thickness, and tube length of the R-TNTs measured from FESEM images was approximately 80 nm, 9 nm, and 4 μm, respectively. The geometrical size of the nanotubes tended to reduce after electrochemical reduction, but the structure of the nanotubes was still intact. The nanotubes were highly ordered, vertically aligned, and covered a large area of the Ti substrate. The color change, from dark grey to black, of the TNTs and R-TNTs could be observed by the naked eye. This phenomenon was due to the presence of Ti^{3+} and an increase in defect density during the reduction process [20–22].

Figure 2 displays the XRD pattern of the as-anodized TNTs and R-TNTs. The XRD patterns obtained for the TNTs and R-TNTs were barely distinguishable from each other with presence of a single phase of TiO_2 indexed to anatase (JCPDS: 21-1272) except for the peaks at 35.43°, 38.74°, 40.49°, and 53.32° which originated from the Ti metal substrate. The crystallite size was calculated using the Debye-Scherrer equation:

$$d = \frac{0.89\lambda}{\beta \cos\theta}, \tag{2}$$

where d is the crystallite size, λ is the wavelength of the Cu K_α radiation (1.542 Å), θ is the Bragg diffraction angle,

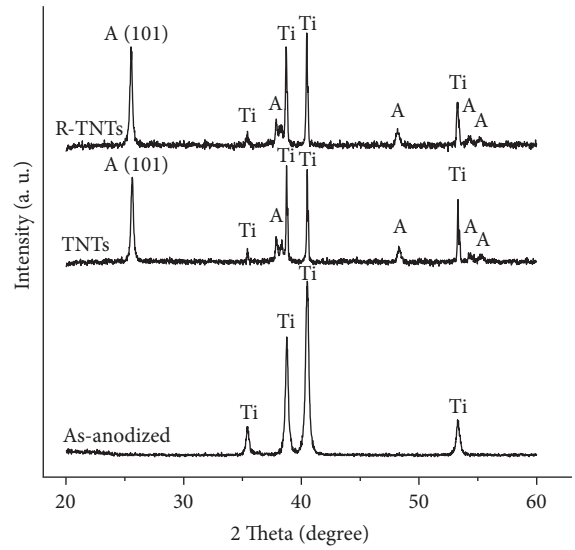

Figure 2: XRD patterns of as-anodized TNTs and R-TNTs.

and β is the full width of the half maximum (FWHM) of the diffraction peak. The crystallite sizes for the TNTs and R-TNTs samples were 35 nm and 38 nm, respectively, based on the (101) plane. From the data, there were no phase changes observed in XRD, and the difference in crystallite size was insignificant after the electrochemical reduction.

XPS techniques were employed to further verify the reduction of the samples and to determine the chemical composition and oxidation state of the Ti element in the TNTs and R-TNTs. Figure 3(a) displays the Ti 2p XPS spectra for both samples, which consisted of two broad peaks centered at 459.1 eV and 465.0 eV corresponding to Ti $2p_{1/2}$ and Ti $2p_{3/2}$ peaks of Ti^{4+} for the TNT samples [13, 18, 20]. In comparison, the peaks for the R-TNTs showed a slight negative shift in the binding energy located at 459.0 eV and 464.8 eV, suggesting the presence of Ti^{3+} ions in the lattice [16, 23]. The presence of Ti^{3+} ions was ~13% in R-TNTs, whereas there were no traces of Ti^{3+} detected in TNTs. A comparison survey of the O 1s XPS spectra was carried out for both samples, and the data is displayed in Figure 3(b). A peak centered at 530.3 eV

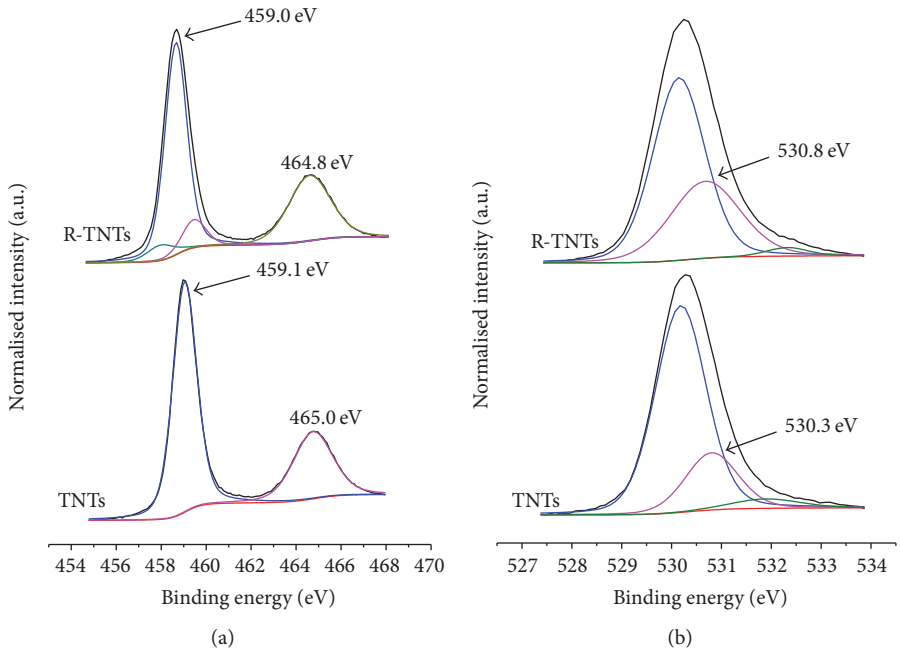

Figure 3: (a) Ti 2p XPS spectra and (b) O 1s XPS spectra of TNTs and R-TNTs.

was seen in both samples, with a higher intensity for R-TNTs. This could be attributed to the presence of the Ti-OH species in the R-TNTs sample. The XPS analysis data suggested that oxygen vacancies were introduced into the R-TNTs lattice during the electrochemical reduction process. The presence of impurities induced by Ti^{3+} and oxygen vacancies in the lattice structure of R-TNTs could possibly enhance the capacitive performance of the samples.

3.2. Electrochemical Measurements. The effect of electrochemical reduction on the capacitive performance of the R-TNTs was investigated via CV, galvanostatic charge-discharge, and EIS measurements. It has been well established that the ideal capacitor exhibits a perfect square when subjected to CV measurements, independently of the scan rate [14, 24]. The shape may slightly transform to a trapezoidal shape as it undergoes a series of resistance and diffusion. Figure 4 shows a comparison of the cyclic voltammograms of TNTs and R-TNTs in a three-electrode configuration collected at a scan rate of 200 mV s^{-1}. In contrast to the TNTs sample which displayed poor electroactivity, the R-TNTs sample displayed an obvious capacitive characteristic curve with no peak associated with a redox reaction [13, 17]. The dramatic increase in the cyclic voltammogram for the R-TNTs, which was approximately 3 times larger than the TNTs, revealed a remarkable improvement in the capacitive performance of the R-TNTs. Besides, the nearly rectangular-shaped cyclic voltammogram possessed by the R-TNTs was as expected for an ideal capacitor [25, 26]. The data indicated that the R-TNTs sample achieved a specific capacitance of 2.81 mF cm^{-2} at a scan rate of 200 mV s^{-1}, which was 18 times higher than the unmodified TNTs (0.16 mF cm^{-2}). This enhancement was attributed to the improvement in electrical conductivity of the samples which led to an enhancement of

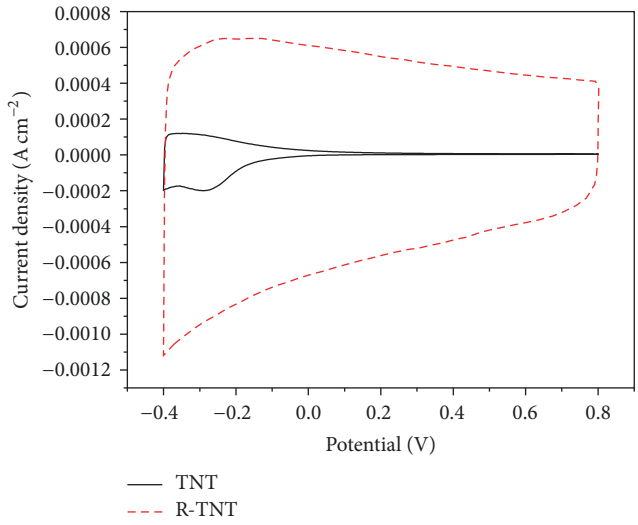

Figure 4: Cyclic voltammograms of TNTs and R-TNTs at a scan rate of 200 mV.

the carrier density, while the existence of oxygen vacancies in the R-TNTs boosted the electrochemical activity of the sample [18]. The possible chemical processes for the formation of oxygen vacancies in the TNTs lattice are as follows:

At the Anode

$$2H_2O \longrightarrow O_2 + 4H^+ + 4e^- \quad (3)$$

At the Cathode

$$TiO_2 + 4H^+ + e^- \longrightarrow Ti^{3+} + 2H_2O \quad (4)$$

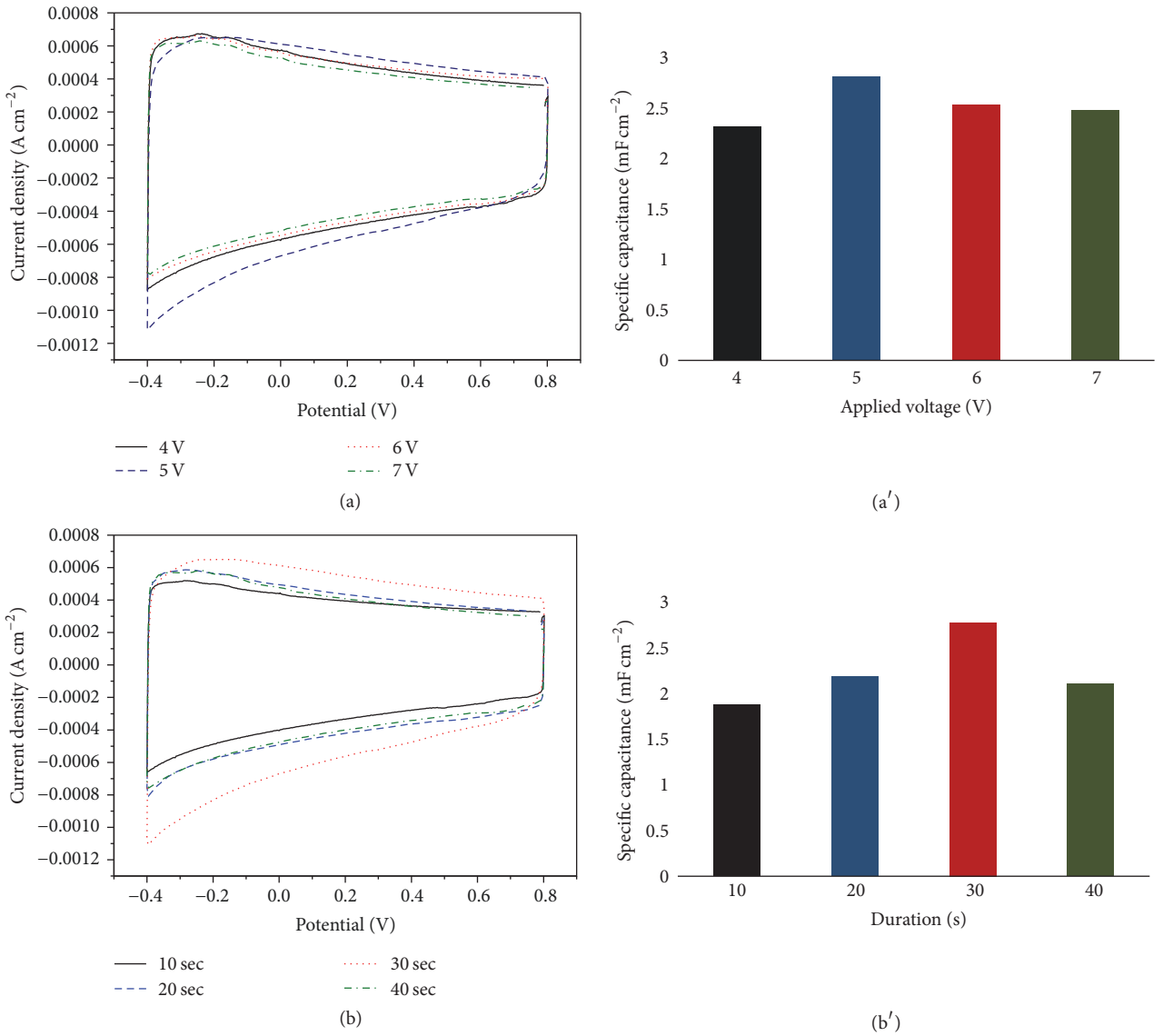

FIGURE 5: Cyclic voltammograms of R-TNTs prepared at different (a) voltage and (b) time, conducted at a scan rate of 200 mV s^{-1}, specific capacitance of R-TNTs with respect to (a′) voltage and (b′) time.

Overall Reaction

$$4TiO_2 + 12H^+ \longrightarrow 4Ti^{3+} + 6H_2O + O_2 \quad (5)$$

Further investigations to find the optimum conditions for the electrochemical reduction process were carried out by varying the voltage and time as listed in Table 1. Based on the FESEM images in Figures 1(a) and 1(b), the R-TNTs samples were stable and did not undergo any destruction or damage after the electrochemical reduction. The cyclic voltammograms of the R-TNTs 4V30s, R-TNTs 5V30s, R-TNTs 6V30s, and R-TNTs 7V30s as shown in Figure 5(a) have displayed a rectangular shape, suggesting typical capacitive behaviour. The specific capacitance of the samples increased as the applied voltage of the electrochemical reduction increased from 4 V to 5 V, followed by a slight drop at higher applied voltages of 6 V and 7 V as depicted in Figure 5(a′). A short circuit error was detected in the DC device at higher applied voltage during the electrochemical reduction which could have caused damage to the films and thus contributed to lower capacitive performance. The cyclic voltammograms of the R-TNTs samples prepared at different electrochemical reduction times (10 s to 40 s with an applied potential of 5 V) in Figure 5(b) displayed an increment in the integrated area for the samples from 10 s to 30 s. However, the cyclic voltammogram was reduced for the sample at 40 s. Figure 5(b′) shows the overall variation of the specific capacitance with increasing time of electrochemical reduction at 5 V. Longer electrochemical reduction times caused the specific capacitance to decrease which was attributed to an increase in the surface defect density and the corresponding recombination rate [14]. The optimum voltage and time for the electrochemical reduction of TNTs for the highest capacitive performance were at 5 V and 30 s, respectively.

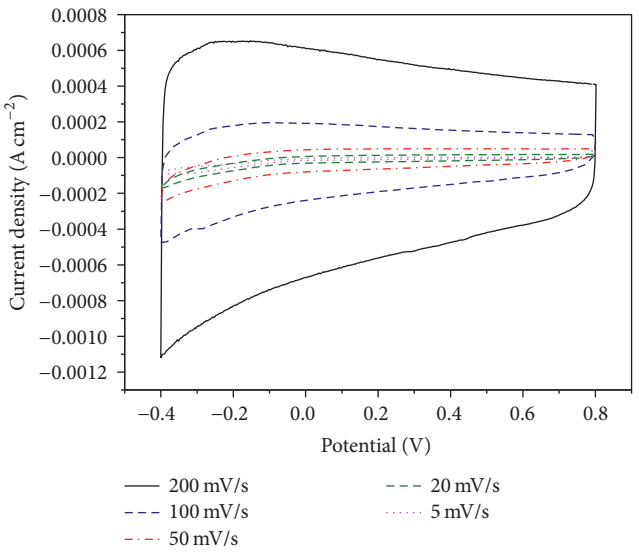

Figure 6: Cyclic voltammograms of R-TNTs recorded at different scan rates from 5 to 200 mV s^{-1}.

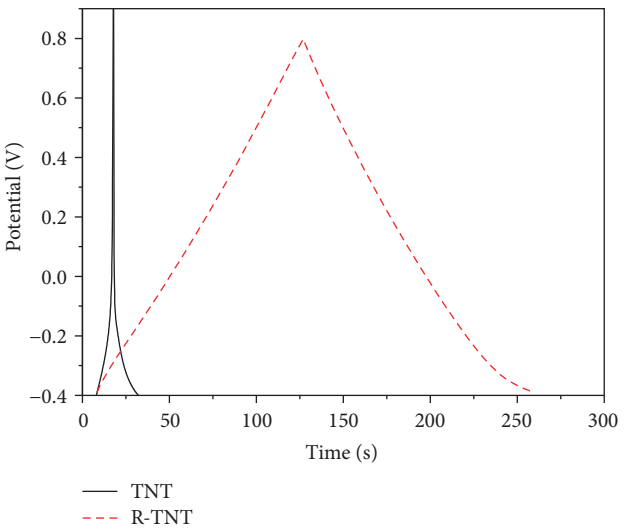

Figure 7: Galvanostatic charge-discharge curves of the TNTs and R-TNTs conducted at a current density of 30 μA cm^{-2}.

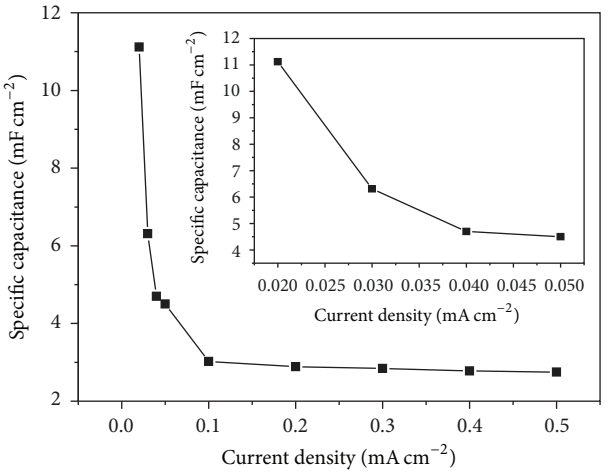

Figure 8: Specific capacitance of R-TNTs at various discharge current densities.

Figure 6 shows the current density versus potential profiles at different scan rates for the R-TNTs 5V30s (denoted as R-TNTs for further discussion) sample. The cyclic voltammograms maintained their rectangular profiles indicating a capacitive charge storage mechanism. As the scan rate increased, the integrated area became larger, which gradually decreased at a lower scan rate. It is postulated that at a higher scan rate, the electron flow increased, which led to the rapid charging of the sample. Thus, a smaller integrated area was observed at a low scan rate. This meant that the R-TNTs could stand extreme cycling conditions.

The charging-discharging curves for the TNTs and R-TNTs conducted at a current density of 30 μA cm^{-2} are displayed in Figure 7 for comparison purposes. The charge-discharge curve of the R-TNTs was symmetric and covered a significantly longer time than the TNTs sample, revealing a good capacitive behaviour. The R-TNTs sample delivered a remarkable improved specific capacitance of 6.31 mF cm^{-2} at the same current density of 30 μA cm^{-2}, which was approximately 57 times higher than the TNTs. The specific capacitance values of both samples were profoundly influenced by the current density. As was observed in Figure 8, the capacitance decreased with increasing current density. At the lowest current density of 20 μA cm^{-2}, the R-TNTs sample delivered an average specific capacitance of 11.12 mF cm^{-2}, while at the highest current density of 500 μA cm^{-2}, a specific capacitance of 2.78 mF cm^{-2} was obtained. This proved that the R-TNTs sample exhibited excellent rate capability at high current density.

Specific capacitance and coulombic efficiency values with respect to the charge-discharge cycle numbers at a constant current density of 10 μA cm^{-2} for the TNTs and 200 μA cm^{-2} for the R-TNTs are plotted in Figures 9(a) and 9(b). This analysis was performed in order to evaluate the stability of the samples under long cycling conditions of up to 1000 cycles. As the cycle number increased, the specific capacitance of the TNTs samples decreased, while the R-TNTs sample exhibited an insignificant difference in the observed capacitance values. The initial specific capacitance of the TNTs with a value of 0.19 mF cm^{-2} declined by about 47% to approximately 0.09 mF cm^{-2}. In comparison to the TNTs, the R-TNTs samples revealed excellent cycle stability in this analysis with retention of 99%. It is worth highlighting that the electrochemically reduced sample exhibited better electrochemical stability and enhanced capacitance behaviour compared to the unmodified TNTs. The coulombic efficiency was calculated based on the following equation:

$$\eta = \left[\frac{t_D}{t_C}\right] \times 100, \quad (6)$$

where t_C and t_D represent the charging and discharging times, respectively. The coulombic efficiency for the R-TNTs

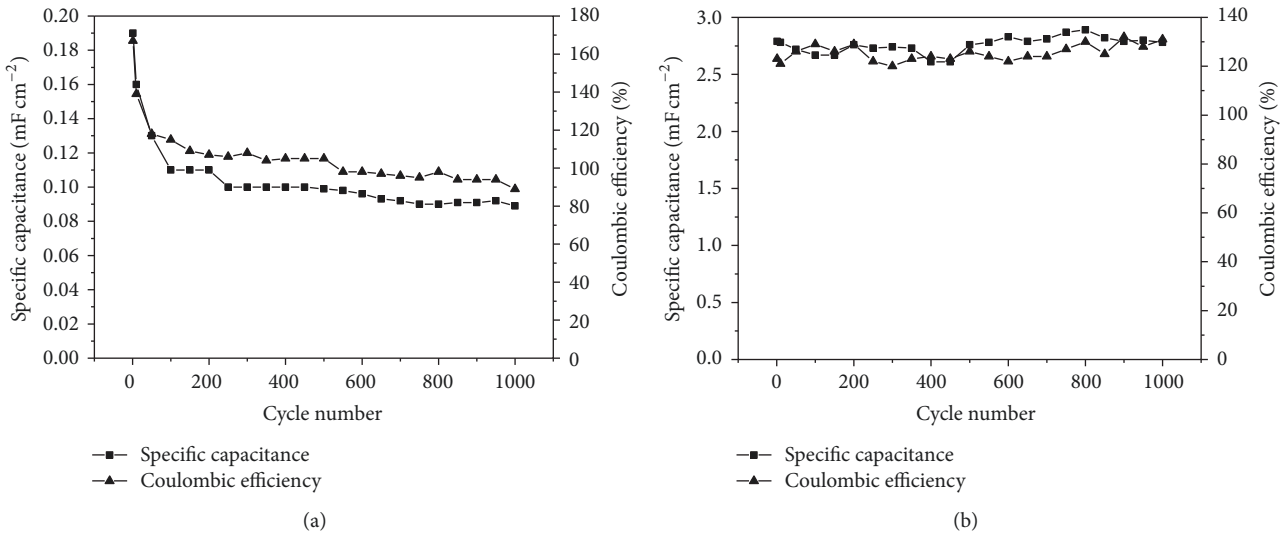

FIGURE 9: Variation of specific capacitance of (a) TNTs and (b) R-TNTs with respect to charge-discharge cycle numbers investigated in 1.0 M KCl at a current density of 10 μA cm^{-2} for TNTs and 200 μA cm^{-2} for R-TNTs.

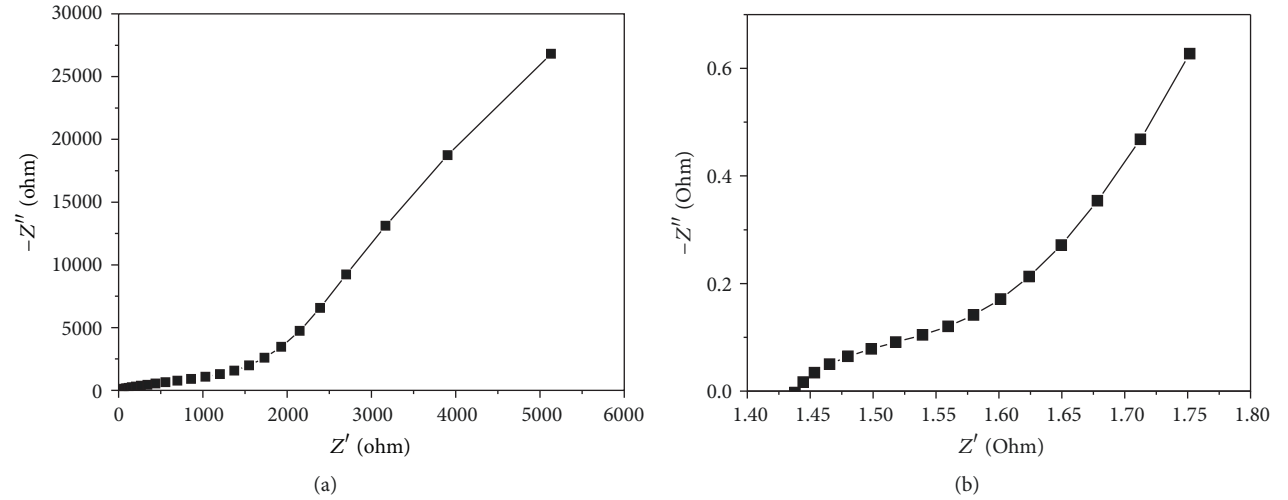

FIGURE 10: Nyquist plots for (a) TNTs and (b) R-TNTs samples.

sample remained at a high plateau indicating that the electrochemical reaction involved at the films-electrolytes interface was fast and reversible which supported the cycle stability data that was discussed previously.

Electrochemical impedance analysis (EIS) is performed to study the resistance behaviour of the samples under alternating current. From the Nyquist plots in Figures 10(a) and 10(b), the TNTs and R-TNTs samples displayed two important features: cell-electrolyte resistance (R_s) and charge-transfer resistance (R_{ct}). R_s is the first intercept of the semicircle formed at the lower part of the plot that corresponds to the high frequency region. The charge-transfer resistance (R_{ct}) at the interface between the electrode and electrolyte was directly acquired from the diameter of the semicircle. Both samples exhibited a semicircle arc characteristic where cell-electrolyte resistance (R_s) and charge-transfer resistance (R_{ct}) values were determined using an electrochemical circle fit. The R_s values for the TNTs and R-TNTs were 2.50 Ω and 1.44 Ω, respectively, as shown in Table 2. The R-TNTs sample recorded the lowest R_s value as a result of the oxygen vacancies in the R-TNTs facilitating an efficient excess of electrolyte ions within the R-TNTs surface, thus enhancing the ion diffusion pathways. In addition, the R-TNTs also recorded a lower R_{ct} value of 1.74 Ω compared to the TNTs, with a value of 790 Ω, and this led to the interpretation of higher specific capacitance. The data obtained was supported by CV and galvanostatic charge-discharge analyses.

4. Conclusions

A fast and simple electrochemical reduction method in an aqueous electrolyte has been presented in this work in order to enhance the capacitive performance of TNTs as a supercapacitor. The reduction of the samples was verified

Table 2: Cell-electrolyte resistance (R_s) and charge-transfer resistance (R_{ct}) obtained from impedance analysis.

Samples	R_s (Ω)	R_{ct} (Ω)
TNTs	2.50	790
R-TNTs	1.44	1.74

with XPS analysis which confirmed the presence of Ti^{3+} in the R-TNTs lattice. It is postulated that the presence of Ti^{3+} and oxygen vacancies due to the reduction process enhanced the conductivity and electrical performance of the sample, hence improving the electrochemical properties of the sample. Ultrahigh conductivity could cause lowered resistance in the samples which led to higher capacitive performance. The R-TNTs exhibited an excellent capacitive performance of 11.12 mF cm^{-2} at 20 μA cm^{-2} and 2.78 mF cm^{-2} at 500 μA cm^{-2}, which was approximately 57 times higher than TNTs. The cyclic voltammogram of the R-TNTs displayed a perfect rectangular shape with no evidence of faradic reaction. The outstanding chemical stability of the R-TNTs sample was confirmed by the galvanostatic charge-discharge test as the sample still possessed 99% capacitive retention after 1000 cycles. Thus, the promising properties of the R-TNTs presented here make it potentially applicable for other technical applications including energy storage as a supercapacitor.

Conflicts of Interest

The authors declare that there are no conflicts of interest regarding the publication of this paper.

Acknowledgments

The authors thank the Ministry of Higher Education of Malaysia (KPT) for financial support and the MyBrain15 scholarship for Nurul Asma Samsudin. Special thanks are extended to the Microscopy Unit, Institute of Biosciences, Universiti Putra Malaysia, MIMOS Failure Analysis Lab, MIMOS Berhad, and the School of Chemistry and Environment, Faculty of Applied Sciences, Universiti Teknologi MARA, for the provision of laboratory facilities.

References

[1] R. J. Brodd, K. R. Bullock, R. A. Leising, R. L. Middaugh, J. R. Miller, and E. Takeuchi, "Batteries, 1977 to 2002," *Journal of The Electrochemical Society*, vol. 151, no. 3, pp. K1–K11, 2004.

[2] P. Kurzweil, "Capacitors: Electrochemical double-layer capacitors," *Encyclopedia of Electrochemical Power Sources*, pp. 634–648, 2009.

[3] A. K. Shukla, S. Sampath, and K. Vijayamohanan, "Electrochemical supercapacitors: Energy storage beyond batteries," *Current Science*, vol. 79, no. 12, pp. 1656–1661, 2000.

[4] Y. C. Eeu, H. N. Lim, Y. S. Lim, S. A. Zakarya, and N. M. Huang, "Electrodeposition of polypyrrole/reduced graphene oxide/iron oxide nanocomposite as supercapacitor electrode material," *Journal of Nanomaterials*, vol. 2013, Article ID 653890, 6 pages, 2013.

[5] P. Kurzweil, "Capacitors: Electrochemical metal oxides capacitors," *Encyclopedia of Electrochemical Power Sources*, pp. 665–678, 2009.

[6] N. A. Samsudin, Z. Zainal, H. N. Lim et al., "Titania nanotubes synthesised via the electrochemical anodisation method: Synthesis and supercapacitor applications," *Pertanika Journal of Scholarly Research Reviews*, vol. 2, pp. 107–128, 2016.

[7] M. Salari, M. Rezaee, S. P. H. Marashi, and S. H. Aboutalebi, "The role of the diluent phase in the mechanochemical preparation of TiO2 nanoparticles," *Powder Technology*, vol. 192, no. 1, pp. 54–57, 2009.

[8] T. Stergiopoulos, A. Ghicov, V. Likodimos et al., "Dye-sensitized solar cells based on thick highly ordered TiO2 nanotubes produced by controlled anodic oxidation in non-aqueous electrolytic media," *Nanotechnology*, vol. 19, no. 23, 2008.

[9] J. R. Jennings, A. Ghicov, L. M. Peter, P. Schmuki, and A. B. Walker, "Dye-sensitized solar cells based on oriented TiO_2 nanotube arrays: transport, trapping, and transfer of electrons," *Journal of the American Chemical Society*, vol. 130, no. 40, pp. 13364–13372, 2008.

[10] V. Zwilling, M. Aucouturier, and E. Darque-Ceretti, "Anodic oxidation of titanium and TA_6V alloy in chromic media. An electrochemical approach," *Electrochimica Acta*, vol. 45, no. 6, pp. 921–929, 1999.

[11] F. Hai-Tao, M. Liu, D. W. Wang et al., "Comparison of the rate capability of nanostructured amorphous and anatase TiO2 for lithium insertion using anodic TiO2 nanotube arrays," *Nanotechnology*, vol. 20, 2009.

[12] M. Salari, S. H. Aboutalebi, A. T. Chidembo, K. Konstantinov, and H. K. Liu, "Surface engineering of self-assembled TiO2 nanotube arrays: A practical route towards energy storage applications," *Journal of Alloys and Compounds*, vol. 586, pp. 197–201, 2014.

[13] M. Salari, K. Konstantinov, and H. K. Liu, "Enhancement of the capacitance in TiO2 nanotubes through controlled introduction of oxygen vacancies," *Journal of Materials Chemistry*, vol. 21, no. 13, pp. 5128–5133, 2011.

[14] H. Wu, D. Li, X. Zhu et al., "High-performance and renewable supercapacitors based on TiO2 nanotube array electrodes treated by an electrochemical doping approach," *Electrochimica Acta*, vol. 116, pp. 129–136, 2014.

[15] Z. Endut, M. Hamdi, and W. J. Basirun, "Supercapacitance of bamboo-type anodic titania nanotube arrays," *Surface and Coatings Technology*, vol. 215, pp. 75–78, 2013.

[16] J. M. Macak, B. G. Gong, M. Hueppe, and P. Schmuki, "Filling of TiO2 nanotubes by self-doping and electrodeposition," *Advanced Materials*, vol. 19, no. 19, pp. 3027–3031, 2007.

[17] M. Salari, S. H. Aboutalebi, A. T. Chidembo, I. P. Nevirkovets, K. Konstantinov, and H. K. Liu, "Enhancement of the electrochemical capacitance of TiO 2 nanotube arrays through controlled phase transformation of anatase to rutile," *Physical Chemistry Chemical Physics*, vol. 14, no. 14, pp. 4770–4779, 2012.

[18] X. Lu, G. Wang, T. Zhai et al., "Hydrogenated TiO 2 nanotube arrays for supercapacitors," *Nano Letters*, vol. 12, no. 3, pp. 1690–1696, 2012.

[19] W. Hui, C. Xu, J. Xu et al., "Enhanced supercapacitance in anodic TiO2 nanotube films by hydrogen plasma treatment," *Nanotechnology*, vol. 24, 2013.

[20] X. B. Chen, L. Liu, P. Y. Yu, and S. S. Mao, "Increasing solar absorption for photocatalysis with black hydrogenated titanium dioxide nanocrystals," *Science*, vol. 331, no. 6018, pp. 746–750, 2011.

[21] M. S. Hamdy, R. Amrollahi, and G. Mul, "Surface Ti3+-containing (blue) titania: A unique photocatalyst with high activity and selectivity in visible light-stimulated selective oxidation," *ACS Catalysis*, vol. 2, no. 12, pp. 2641–2647, 2012.

[22] J. Wang, P. Yang, and B. Huang, "Self-doped TiO2-x nanowires with enhanced photocatalytic activity: Facile synthesis and effects of the Ti3+," *Applied Surface Science*, vol. 356, pp. 391–398, 2015.

[23] E. McCafferty and J. P. Wightman, "Determination of the concentration of surface hydroxyl groups on metal oxide films by a quantitative XPS method," *Surface and Interface Analysis*, vol. 26, no. 8, pp. 549–564, 1998.

[24] M. Salari, S. H. Aboutalebi, K. Konstantinov, and H. K. Liu, "A highly ordered titania nanotube array as a supercapacitor electrode," *Physical Chemistry Chemical Physics*, vol. 13, no. 11, pp. 5038–5041, 2011.

[25] E. Frackowiak and F. Béguin, "Carbon materials for the electrochemical storage of energy in capacitors," *Carbon*, vol. 39, no. 6, pp. 937–950, 2001.

[26] P. Simon and Y. Gogotsi, "Materials for electrochemical capacitors," *Nature Materials*, vol. 7, no. 11, pp. 845–854, 2008.